Synthesis, solvatochromism and crystal structure of trans-[Cu(Et₂NCH₂CH₂NH₂)₂.H₂O](NO₃)₂ complex: Experimental with DFT combination

Ismail Warad [a, *], Sharif Musameh [b], Ismail Badran [a, **], Nashaat N. Nassar [c], Paula Brandao [d], Carlos Jose Tavares [e], Assem Barakat [f, ***]

[a] Department of Chemistry, AN-Najah National University, P.O. Box 7, Nablus, Palestine
[b] Department of Physics, AN-Najah National University, P.O. Box 7, Nablus, Palestine
[c] Department of Chemical and Petroleum Engineering, University of Calgary, 2500 University Street NW, Calgary, Alberta, T2N 1N4, Canada
[d] Department of Chemistry, CICECO, University of Aveiro, 3810-193, Aveiro, Portugal
[e] Center of Physics, University of Minho, Campus of Azurem, 4804-533, Guimaraes, Portugal
[f] Department of Chemistry, College of Science, King Saud University, P. O. Box 2455, Riyadh, 11451, Saudi Arabia

ARTICLE INFO

ABSTRACT

In this study, two dicationic asymmetrical diamine/copper(II) nitrate salt complexes of the general formula trans-[Cu^{II}(NN')₂.H₂O](NO₃)₂ were successfully synthesized using N,N-dimethylethylenediamine and N,N-diethylethylenediamine as asymmetrical diamine ligands. The structure of complex **2** was identified by X-ray single crystal diffraction analysis confirming that the bidentate ligand N,N-dimethylethylenediamine forms a penta-coordinated complex with an H₂O molecule located around the copper(II) ion in a trans configuration. It was found that the metal centre is coordinated in a distorted square pyramidal fashion with a τ value of 0.274. The desired complexes were fully characterized using, MS, UV–Vis, CV, FTIR, TG/DTA, and Hirshfeld surface computational analysis. High level theoretical calculations were also performed in order to investigate the complexes structure, conformers, vibrational frequencies, and their excited states.

© 2017 Elsevier B.V. All rights reserved.

1. Introduction

Copper is one of the most authentic transition metal elements in human bodies, where its ion complexes play an essential role in bio-catalytic processing [1–4]. In general, copper(II) complexes behave as good anti-cancer agents due to their affinity to bind to DNA with several types of interactions [4–10]. Hence, a large number of copper(II) complexes have been synthesized and evaluated as DNA binders and anti-cancer drugs [11–23].

The implementation of five-coordinated Cu(II) complexes with two diamine ligands are widespread in coordination chemistry [21–23]. The structural, electronic and stereochemistry of such complexes have been discussed extensively [21–24]. The geometry of five-coordinate complexes ranges between square pyramidal (SP) and trigonal bipyramidal (TBP). Very few copper(II) complexes with regular TBP geometry are known, with the exception of some complexes containing tripodal ligands [24].

The coordination chemistry of diamines ligands with copper(II) complexes has attracted attention considering their important catalytic, structural, magnetic and biological properties [25,26]. Only a small number of asymmetric diamines ligands with alkyl nitrogen atom (R₂N) and aprotic nitrogen atom (H₂N), such as N,N-dimethylethylenediamine have been investigated in Cu(II) complexation. Coordination of two asymmetrical diamine ligands with Cu(II) centre with five-coordinated orientation may favour the trans structure as a kinetically-favoured isomer or the cis structure as a thermodynamically-favoured isomer. To the best of our knowledge, the cis/trans isomerization of asymmetric diamines to the Cu(II) centre has never been theoretically studied.

In the literature, there are numerous number of copper(II)/N-donors complexes; which are being used mainly as DNA binders [1–4,21–24]. However, there is a shortage in the X-ray single-

* Corresponding author.
** Corresponding author.
*** Corresponding author.
  E-mail address: warad@najah.edu (I. Warad).

crystal diffraction (XRD) of such complexes. In addition, theoretical calculations on such complexes are very rare. In this work, the crystal structure of the *trans*-[Cu^{II}(NN′)$_2$.H$_2$O](NO$_3$)$_2$ isomer (complex **2**) was successfully prepared and isolated. The structure was analysed with the means of single-crystal XRD, FTIR, and UV–vis. In addition, high level computational calculations were performed in order to study the structure, the *cis/trans* isomerization, and the vibrational spectra of the copper(II)/diamines complexes. Time-dependent DFT (TDDFT) methods were also used to probe the excitation states of the complexes and compare their UV–vis spectra to the experimental ones.

2. Experimental section

2.1. Materials

All the reagents that were used are of analytical grade and purchased from Sigma–Aldrich and used as received.

2.2. Synthetic procedure

1 mmol of Cu(NO$_3$)$_2$·3H$_2$O was dissolved in 10 ml of methanol. Then, 2.1 mmol of the corresponding diamine ligand dissolved in 5 ml of methanol was added drop by drop under ultrasound waves to the Cu(II) solution until the solution turned dark blue in a period ~ 20 min. After that, the solvents were removed under vacuum at 65 °C and the remaining solid was washed with chloroform (to remove excessive amines) and dried under vacuum. Crystals from complex **2** suitable for X-ray diffraction were obtained through slow evaporation of water from the solution of the complexes.

2.2.1. [Cu(Me$_2$NCH$_2$CH$_2$NH$_2$)$_2$·H$_2$O](NO$_3$)$_2$ (1)
Blue water soluble powder with 83% yield, m. p. = 185 °C. MS *m/z* 227.2 [M-2NO$_3$]$^+$ for C$_6$H$_{20}$CuN$_5$O$_7$ Calculated: C, 20.48; H, 5.73; N, 23.89. Found C, 20.33; H, 5.62; N, 23.71%, IR (KBr, νcm^{-1}): 3240 (ν$_{H2O}$), 3180 and 3140(ν$_{H-N}$), 2930 (ν$_{C-H}$), 1150 (ν$_{N-C}$), 520 (ν$_{Cu-N}$). UV–vis in water: λ_{max} (ε_{max}/M^{-1} cm^{-1}): 250 nm (1.15 × 10^4 M^{-1}L^{-1}) and 565 nm (8.20 × 10^2 M^{-1}L^{-1}).

2.2.2. [Cu(Et$_2$NCH$_2$CH$_2$NH$_2$)$_2$·H$_2$O](NO$_3$)$_2$ (2)
Blue water soluble powder with 85% yield, m. p. = 182 °C. Yield 90%, m. p. = 182 °C. MS *m/z* 266.1 [M-2NO$_3$]$^+$ for C$_8$H$_{24}$CuN$_5$O$_7$ Calculated: C, 25.30; H, 6.37; N, 22.12. Found C, 25.15; H, 6.12; N, 22.08%, IR (KBr, νcm^{-1}): 3230 (ν$_{H2O}$), 3160 and 3150(ν$_{H-N}$), 2910 (ν$_{C-H}$), 1140 (ν$_{N-C}$), 520 (ν$_{Cu-N}$). UV–vis in water: λ_{max} (ε_{max}/M^{-1} cm^{-1}): 260 nm (1.50 × 10^4 M^{-1}L^{-1}) and 598 nm (8.50 × 10^2 M^{-1}L^{-1}).

2.3. Characterizations

Elemental analyses were recorded with an Elementar Varrio EL analyser. The FTIR spectra (4000–400 cm^{-1}) were obtained from sample powders dispersed in KBr discs with a Perkin–Elmer 621 spectrophotometer. Thermal analyses were carried out with TA instrument SDT-Q600 in air. Absorption spectra were recorded in water at room temperature, on a Pharmacia LKB-Biochrom 4060 spectrophotometer. FAB-MS data were obtained with a Finnigan 711A (8 kV), modified by AMD and reported as mass/charge (*m/z*) values.

2.4. Single-crystal X-Ray data collection

The X-ray single crystal data of complex **2** was collected with monochromated Mo-Kα radiation (λ = 0.71073 Å) on a Bruker SMART Apex II diffractometer equipped with a CCD area detector at 150(2) K. The crystal was positioned at 40 mm from the CCD and the spots were measured using 20 s counting time. Data reduction was carried out using the SAINT-NT software package [27]. Multi-scan absorption correction was applied to all intensity data using the SADABS program [28]. The structure was solved by a combination of direct methods with subsequent different Fourier syntheses and refined by full matrix least squares on F^2 using the SHELX-2013 suite [29]. All non-hydrogen atoms were refined with anisotropic thermal displacements. The C–H hydrogen atoms were included at calculated positions and refined with isotropic parameters equivalent 1.2 times those of the atom to which they are attached. Furthermore, the hydrogen atoms bound to nitrogen atom as well for coordinated water molecule were unequivocally located from the last calculated difference Fourier maps.

The molecular and packing diagrams were generated using the Platon and *Olex2* software [30]. The details of the crystal structure and data refinement are given in Table 1. The list of bond lengths and bond angles of the non-hydrogen atoms are given in Table 2. Fig. 1 represents the ORTEP of the molecule with thermal ellipsoids drawn at a 50% probability.

2.5. Theoretical calculations

Exact details on performing the quantum computational calculations are described in previous studies [31,32]. The copper complexes studied in this work were optimized to their equilibrium geometries and characterized by the analytical calculation of their harmonic frequencies. In order to describe the copper-complex structures obtained experimentally, two families of computational methods were tested. First, the density functional theory (DFT) was employed using the hybrid functional, BHandH and B3LYP [33] and the 6-31 + G(2d,p) basis set. The second computational method was based on using the effective core potential (ECP). This was done by describing the transition metal with three different basis sets, SDD [34] LANL2DZ and Def2TZVPP [35] and all other atoms (H, C, N, and O) by the 6-311 + G(2d,p) basis set. Zero-point energies (ZPE) were scaled by a factor of 0.9748 as suggested by Scott and Radom [36]. Because of the Cu-complexes used in this work were cations, the open shell unrestricted spin was requested by adding the prefix u to the method, i.e., uB3LYP, or uBHandH. In order to locate the most stable structure among the different conformers of the Cu-complexes, single point energies were requested after complete optimization using the Møller−Plesset perturbation theory (MP2) [37] provides using the 6-311++g(2d,p) basis set. For

Table 1
Crystal data and structure refinement for complex **2**.

Empirical Formula	C$_{12}$H$_{34}$CuN$_6$O$_7$
M$_w$	437.99
Crystal system	Monoclinic
Space group	*C2/c*
a/[Å]	15.1603(14)
b/[Å]	8.3978(10)
c/[Å]	16.1732(16)
B/°	105.251(4)
V [Å^3]	1986.5(4)
Z	4
D$_c$ [Mg m^{-3}]	1.464
μ/[mm^{-1}]	1.145
F(000)	932
Crystal size [mm]	0.18 × 0.16 × 0.08
Reflections collected	14258
Unique reflections, [R$_{int}$]	2196 [0.0376]
R$_1$, wR$_2$ [I > 2σI]	0.0281, 0.0631 [1908]
R$_1$, wR$_2$ (all data)	0.0357, 0.0660
Data/restraints/parameters	2195/133/1
Goodness-of-fit on F^2	1.080

Table 2
Selected bond distances (Å) and bond angles (°) for complex **2**.

Bond lengths			
Cu−N(1)	2.010(2)	Cu−N(1i)	2.010(2)
Cu−N(2)	2.105(2)	Cu−N(2i)	2.105(2)
Cu−O(1)	2.225(2)		
Bond angles			
N(1)−Cu−N(2)	84.64(6)	N(2)−Cu−N(2i)	156.89(9)
N(1)−Cu−N(1i)	173.34(11)	N(1)−Cu−O(1)	86.67(6)
N(1)−Cu−N(2i)	96.70(6)	N(1i)−Cu−O(1)	86.67(6)
N(1i)−Cu−N(2)	96.70(6)	N(2)−Cu−O(1)	101.56(4)
N(1i)−Cu−N(2i)	84.64(6)	N(2i)−Cu−O(1)	101.56(4)

i = 1-x,y,3/2-z.
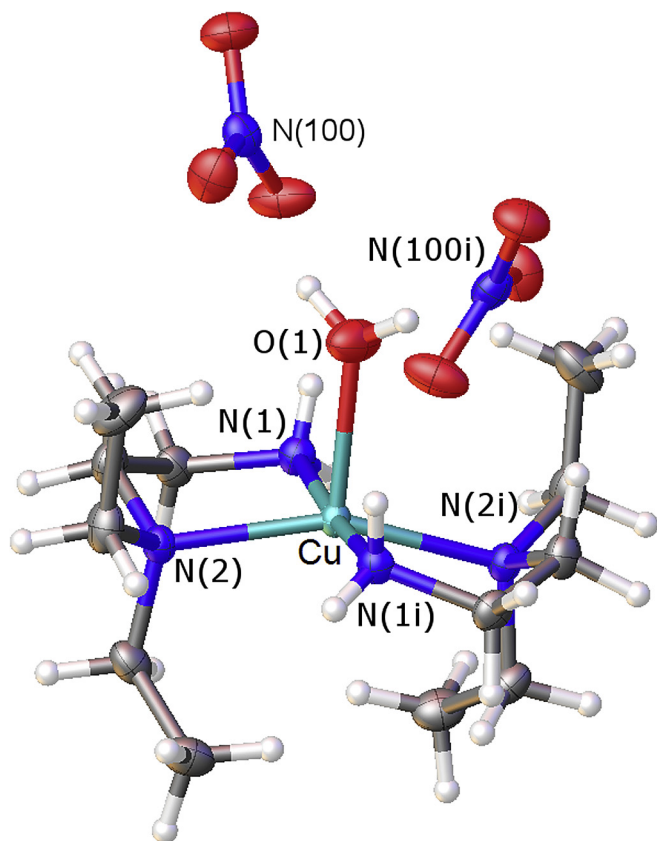
Fig. 1. Molecular structure of complex **2** with thermal ellipsoids drawn at 50% probability level.

the calculations involving solvents, the SCRF method was used. Time-dependent density functional theory calculations used for probing the excited states of the Cu-complexes were performed at uBHandH/6-31 + g(2d,p) level of theory. All electronic calculations

in this work were performed using the Gaussian 09 program [38]. Hirshfeld surfaces and the associated 2D-fingerprint plots were calculated using Crystal Explorer [39].

3. Results and discussion

3.1. Synthesis of Cu(II) complexes

Two new dicationic water-soluble *trans*-[Cu(NN')$_2$.H$_2$O](NO$_2$)$_2$ complexes were synthesized by using *N,N*-dimethylethylenedi-amine and *N,N*-diethylethylenediamine as asymmetrical diamine ligands in methanoic medium and under ultrasonic wave atmosphere (Scheme 1).

The desired complexes have been isolated as NO$_3$ salts in good yields. The complexes are soluble in water, MeOH, DMF and DMSO. However, they are totally insoluble in THF, acetone, CH$_2$Cl$_2$ and non-polar solvents like n-hexane. The solubility and conductivity measurements have confirmed the dicationic nature of the complexes. The progress of the synthesis was followed by colour changes (from brown to sky blue). The prepared complexes have been characterized using elemental analysis, MS, TG/DTA and spectroscopic methods. The X-ray crystal structure of complex **2** revealed a distorted trigonal bipyramidal environment.

P. Naumov deposited complex **2** structure (CCDC 616566) with 6.75 R-value, the authors did not do any structure descriptions or a calculation, the complex was used to enhance adsorption, nothing else was reported [40]. In our case we deposited complex **2** structure (CCDC 1529101) with better 2.81 R-value, both the crystal information data (cif files) of the complex were used to evaluate the experimental and calculated structure parameters.

3.2. Crystal structure and ab-initio calculations of complex 2

As per the single crystal analysis, complex **2** was crystallized in the Monoclinic structure with *C2/c* space group. The crystal data and the structure refinement parameters are given in Table 1, and selected bond distances and angles are given in Table 2. The ORTEP diagram of the complex with the atomic numbering is also shown in Fig. 1.

The coordination geometry around the Cu(II) centre can be described as a distorted square pyramidal towards a trigonal bipyramidal arrangement by a τ value of 0.274. This trigonal index was calculated using the formula $\tau = (\beta - \alpha)/60$ as previously defined by Addison et al. [41], with τ assuming values between 0 and 1 for ideal square pyramidal and trigonal bipyramidal geometries, respectively. In complex **2**, β and α correspond to N(1)−Cu−N(1)i and to N(2)−Cu−N(2i) angles, respectively. The equatorial coordination of copper centre is composed of four nitrogen atoms from the diamine ligand.
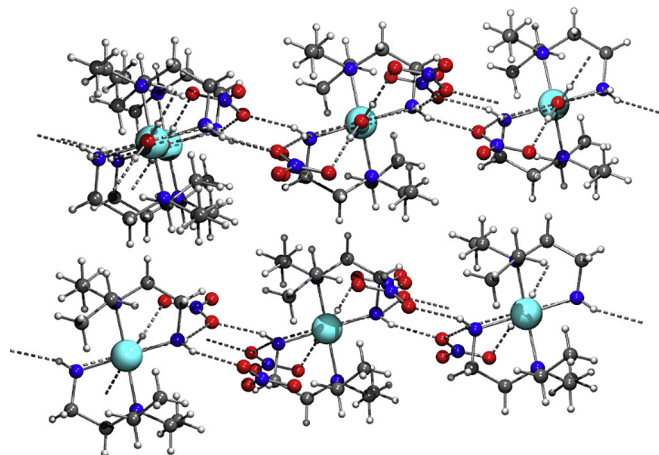
As shown in Fig. 1, the water molecule occupies the apical pyramidal position with the oxygen atom located at 2.225(2) Å from the copper centre. The Cu−N distances of 2.010(2) and 2.105 (2) Å as

R = Me (complex **1**) or Et (complex **2**)   **trans**   **cis**
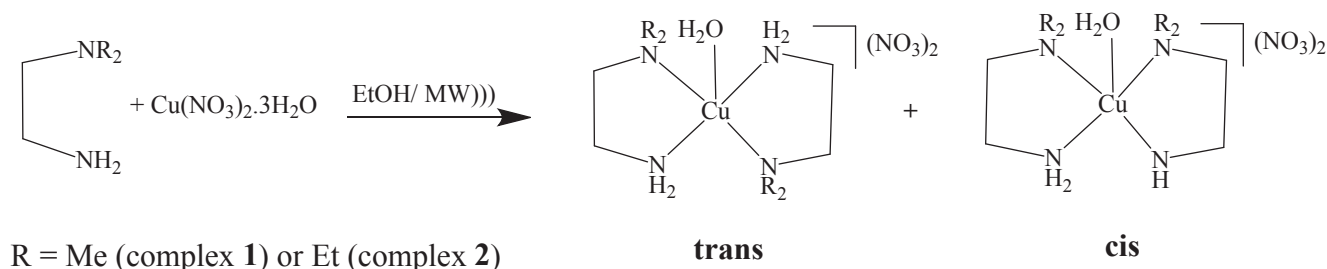
Scheme 1. Synthesis of copper(II) complexes **1** and **2**.

Table 3
Hydrogen bond dimensions for complex **2**.

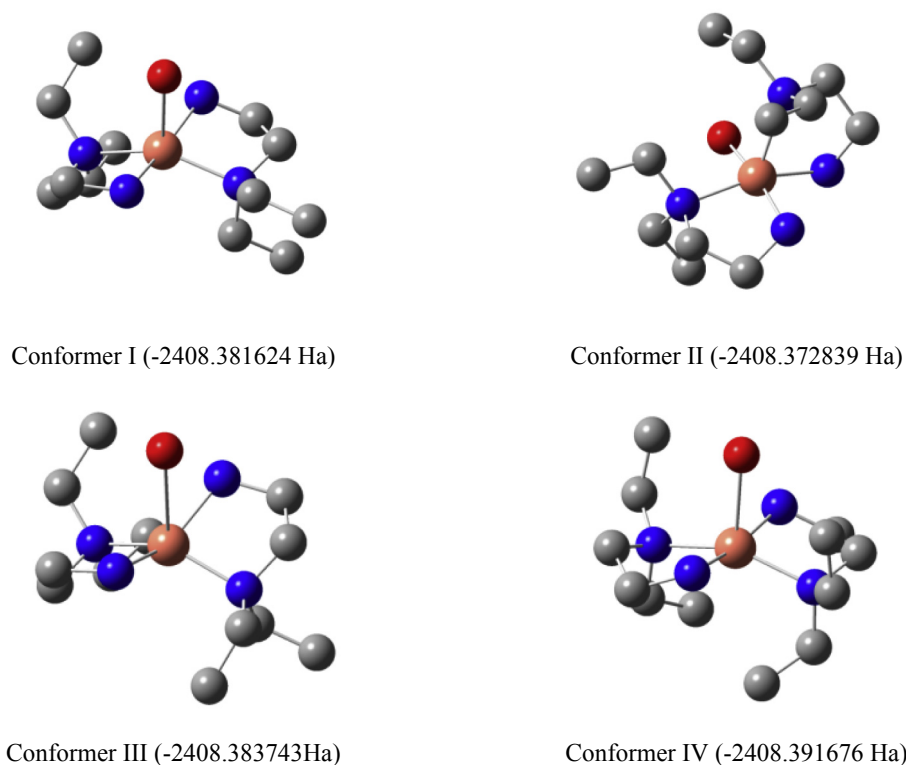| D—H···A	H···A/Å	D···A/Å	D—H···A/°
O(1)—H(1)···N(100)	2.54(2)	3.336(2)	154
[-x + 1,y,-z + 3/2]			
O(1)—H(1)···O(101)	1.81(3)	2.672(2)	177
[-x + 1,y,-z + 3/2]			
N(1)—H(1C)···O(102)	2.27(2)	3.056(2)	157
N(1)—H(1D)···O(102)	2.26(2)	3.063(2)	162
[-x + 3/2,y-1/2,-z + 3/2]			
N(1)—H(1D)···O(103)	2.638	3.222(2)	128
[-x + 3/2,y-1/2,-z + 3/2]			

Fig. 2. Crystal packing diagram of complex **2**, view along [010] crystallographic direction. The dotted lines indicate inter-molecular hydrogen bonds.

well as the Cu—O distance of 2.225(2), are within the expected values for copper(II) complexes with diamine type ligands [42].

As revealed from the crystal lattice, the N···O and O···O inter-molecular distances are consistent with the existence of a 2-D dimensional network of N—H···O and O—H···O hydrogen bonding interactions between the $[Cu(NN')_2.H_2O]^{2+}$ cations, and NO_3^- anions. The H-bond interactions are listed in Table 3 and also shown in Fig. 2.

In order to better understand the relative stability of complex **2** isomerization, we performed *ab-initio* calculations on different possible structural arrangements of the complex. Using the BHandH hybrid density functional, different isomers of the complex **2** structure were optimized. The optimization results and the corresponding final energies at BHandH/6-31 + G(2d,p) level of theory are shown in Fig. 3. Interestingly, the distorted square-pyramidal isomer (IV) was found to be the most stable structure, in full agreement with the XRD findings discussed earlier. The isomers I, II, and III were found to be less stable than isomer IV by 6.3, 11.8, and 5.0 kcal/mol, respectively. After verifying the isomer IV to be the most stable structure, different computational methods were tested in order to describe the structural parameters of the complex, as previously described in the theoretical methods section. Table 4 lists the key structural parameters for the complex **2** obtained at the two DFT functional B3LYP and BHandH with the basis set 6-31 + G(2d,p), and the effective core potential (ECP) methods using the basis sets Def2TZVPP, LANL2DZ, and SDD. The table also shows the same structural parameters obtained experimentally by X-ray diffraction. Clearly, the structure optimized by the DFT functional, BHandH, shows the best match to the experimental structure; such finding is in agreement with previous theoretical studies utilizing the BHandH function [43]. Although the ECP methods were recommended to describe transition metal

Conformer I (-2408.381624 Ha)

Conformer II (-2408.372839 Ha)

Conformer III (-2408.383743Ha)

Conformer IV (-2408.391676 Ha)

Fig. 3. Optimized structures and final energies (in hartree) for different isomers of complex **2** obtained at BHANDH/6-31 + G(2d,p) level of theory. C atom, grey; N atom, blue; H atoms are not shown.

Table 4
Structural parameters for complex **2** obtained at different computational level of theories.

Parameter	XRD structure	ECP/Def2TZVPP	Error	ECP/LANL2DZ	Error	ECP/SDD	Error	B3LYP	Error	BHandH	Error
Cu−N1	2.0096	2.0536	2.2%	2.0601	2.5%	2.0465	1.8%	2.0229	0.7%	1.9833	1.3%
Cu−N2	2.1050	2.1645	2.8%	2.1766	3.4%	2.1600	2.6%	2.1611	2.7%	2.0680	1.8%
Cu−N3	2.0097	2.0301	1.0%	2.0365	1.3%	2.0220	0.6%	2.0229	0.7%	1.9833	1.3%
Cu−N4	2.1050	2.1624	2.7%	2.1740	3.3%	2.1579	2.5%	2.1611	2.7%	2.0681	1.8%
Cu−O	2.2249	4.2795	92.3%	4.2801	92.4%	4.2746	92.1%	3.0807	38.5%	2.4033	8.0%

structures, the three ECP basis sets used in this work have failed in optimizing the complex **2** structure, as seen from the large error values in Table 4. The largest errors are associated with the Cu−O bond distance, which was over estimated by the ECP methods, and the N1−N2−N3−N4 dihedral angle.

3.3. Comparison between XRD and DFT structure parameters of complex 2

The crystal information data (cif files) for complex **2** in this work and P. Naumov [40] were used in order to compare the structure parameters like bond lengths and angles with the calculated DFT result. The optimized main angles and bond lengths around the copper centre were compared to experimental data, as seen in Table 5, Figs. 4 and 5. Fig. 4 showed that: plotting the X-ray experimental bonds lengths (this work) against experimental bonds lengths [40] reflected an excellent matching with correlation coefficient $R^2 = 0.9987$ (Fig. 4a), the bonds lengths are semi-identical (Fig. 4d). Plotting of the X-ray experimental bond length (this work) vs. DFT showed better data with $R^2 = 0.8996$ (Fig. 4b), compared to experimental bond lengths [40] $R^2 = 0.8773$ (Fig. 4c). Fig. 5 showed very good angles agreement between experimental with DFT. Fig. 5a reflected graphical correlation with excellent $R^2 = 0.9998$ value when experimental angles (this work) vs. experimental [40] was plotted, semi-identical angles values between experimental were detected (Fig. 5d). Fig. 5b plotting experimental (this work) vs. DFT revealed very high $R^2 = 0.9967$. Fig. 5c, plotting experimental [40] vs. DFT also revealed an excellent $R^2 = 0.9966$.

3.4. Hirshfeld surface analysis of complex 2

Hirshfeld surface analysis is an essential technique for showing packing modes and intermolecular interactions of crystals structure using CIF file output data [44–48]. Complex **2** was subjected to Hirshfeld surface analysis as seen in Figs. 6 and 7.

Fig. 4 shows Hirshfeld surfaces comprising of d_{norm} surface plots, curvedness, and shape index electrostatic potentials of intermolecular interactions and molecular shapes. Different types of intermolecular interactions were identified. The large dark spots on the surface appear as a result of strong hydrogen bond

acceptors near the nitrogen and oxygen of nitrate, which clearly illustrates the presence of both intra and inter molecular H ….N and H ….O hydrogen bonds. Such binding is expected to be strong enough to stabilize the crystalline structure, in which the NO_3 counter ions played a crucial role in stabilizing the molecular crystal structure [40].

Fig. 7 shows 2D fingerprint plots revealed by colour coding distances from the surface to the nearest atom exterior (**de** plots) or interior (**di** plots) to the surface into specific atom … atom contacts in complex **2**. The percentage of contribution of each contact to the Hirshfeld surface shows that the greatest contribution is due to (a) total, (b) H … all (84%), (c) H⋯H (56%), (d) H⋯O (27%), (e) H⋯N (2%) and (f) H⋯C/Cu (0%) contacts as seen in Fig. 4.

### 3.5. Visible and ultraviolet spectral data

The electronic absorption spectra for complexes **1** and **2** were performed in water at 25 °C. Fig. 8 shows the UV−Vis spectra for the two complexes at different concentrations. In the UV-region: complex **1** had one absorption band at $\lambda_{max} = 250$ nm, and complex **2** exhibited also one band at $\lambda_{max} = 260$ nm, which were attributed to π to π* electron transition.

In the visible region, both complexes **1** and **2** exhibit one broad band each at $\lambda_{max} = 560$ and 595 nm, respectively, which can be attributed to d−d electron transfer.

The excitation states for complex **2** were studied by utilizing the time-dependent density functional theory (TDDFT). The first ten excited states of the complex cation are listed in Table 6. The table also lists the excitation energy in units of eV, the wavelength, and the oscillator strength, and the S^2 value for each excited sate. The square multiplicity (S^2) values, which equal S(S+1), for most of the excited sates are close to 0.75, indicating a doublet state. The S^2 values for states 8, 9, and 10 suffer from serious spin contamination. It was noted that the maximum wavelength (λ_{max}) of absorption for complex **2** in the visible region occurs at 598 nm in aqueous solution. According to these calculations, the excitation energies of states 3 and 4 are the closest to the experimental λ_{max}. However, these excited states are forbidden as their oscillator strengths are null. Hence, it is concluded that the second excited state at 606 nm is the one responsible for the experimental λ_{max} of complex **2**.

Table 5
Experimental and DFT structural parameters for complex **2**.

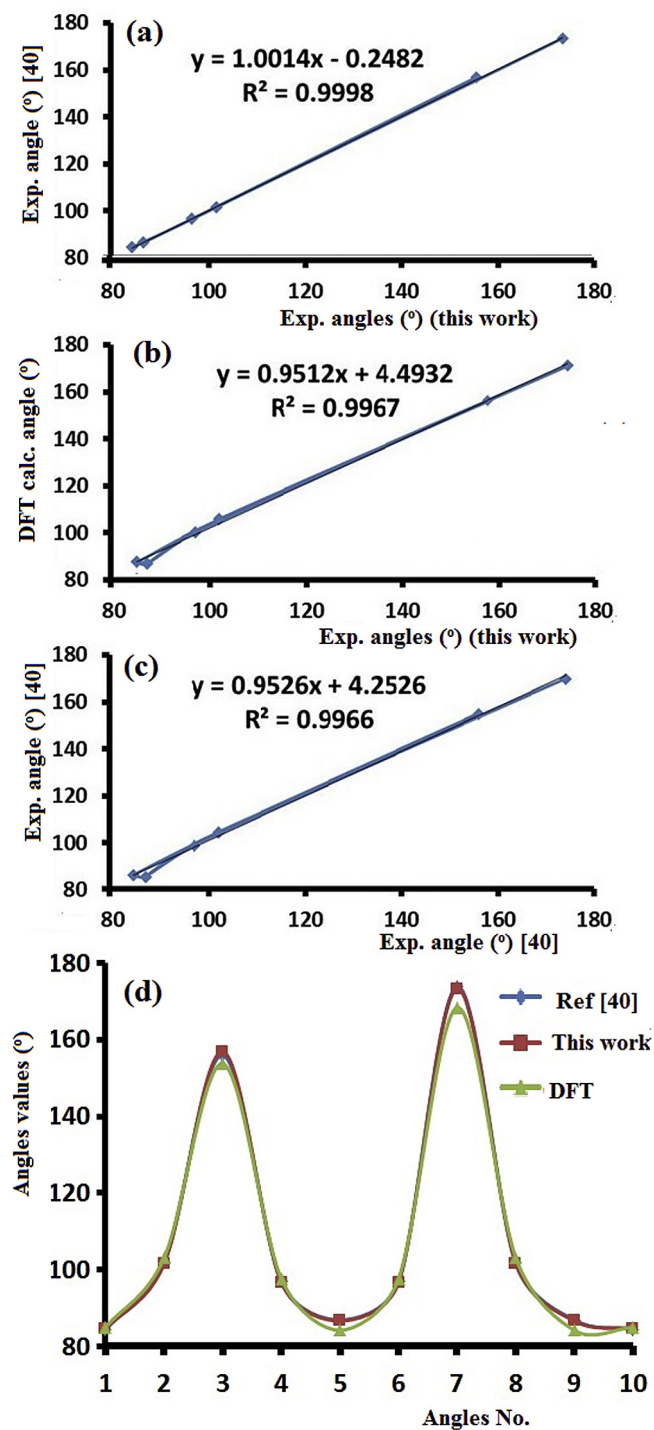| bond No.	Bond type		Bond length			Angle No.	Angle type			Angle value		
			XRD [40]	XRD	DFT					Angle [40]	Angle	DFT
1	Cu1	N1	2.106	2.105	2.068	1	N1	Cu1	N2	84.4	84.64	85
2	Cu1	N2	2	2.01	1.9832	2	N1	Cu1	O4	102	101.56	103.13
3	Cu1	O4	2.226	2.225	2.4084	3	N1	Cu1	N1	156	156.89	153.74
4	Cu1	N1	2.106	2.105	2.068	4	N1	Cu1	N2	96.9	96.7	97.65
5	Cu1	N2	2	2.01	1.9832	5	N2	Cu1	O4	86.9	86.66	84.19
						6	N2	Cu1	N1	96.9	96.7	97.65
						7	N2	Cu1	N2	173.9	173.33	168.37
						8	O4	Cu1	N1	102	101.56	103.13
						9	O4	Cu1	N2	86.9	86.66	84.19
						10	N1	Cu1	N2	84.4	84.64	85
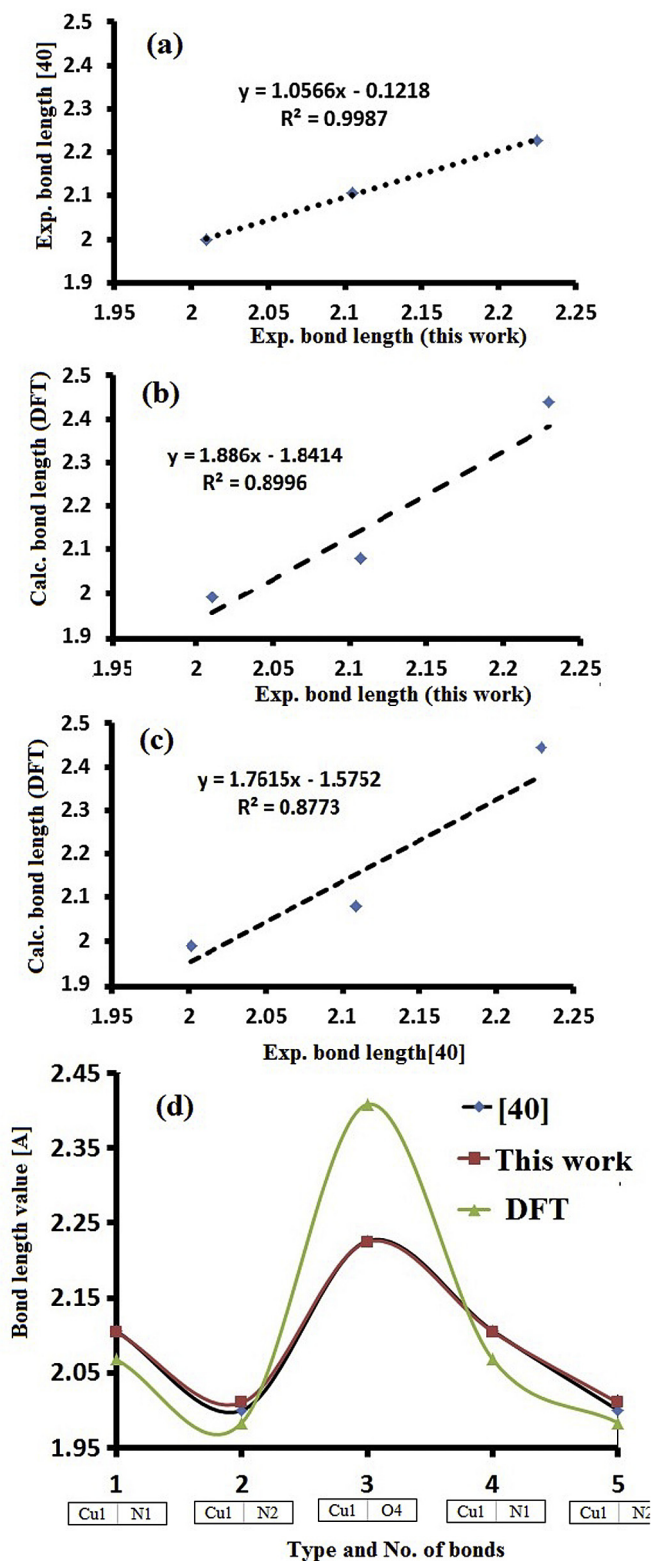
Fig. 4. Graphical correlation of bond lengths (Å): a) experimental this work vs. experimental [40], (b) experimental this work vs. DFT, (c) experimental [40] vs. DFT and (d) bond length vs. bonds types.

Fig. 5. Graphical correlation of angles (°): a) experimental (this work) vs. experimental [40], (b) experimental (this work) vs. DFT, (c) experimental [40] vs. DFT and (d) angles values vs. bonds numbers.

3.6. Solvatochromism

The solubility of complexes in water and polar organic solvents is evident characteristic of solvatochromism, which is equivalent to dicationic mononuclear complexes. The colour sweeping in such complexes are imputed to the d–d electron transition in Cu(II) centre as an outcome of solute-solvent interactions.

The λ_{max} values of the complexes in various solvents were bathochromic shifted depending on polarity of the solvents, as shown in Fig. 9. The polar solvents with heteroatoms are able to coordinate the square pyramidal Cu(II) which may changes the
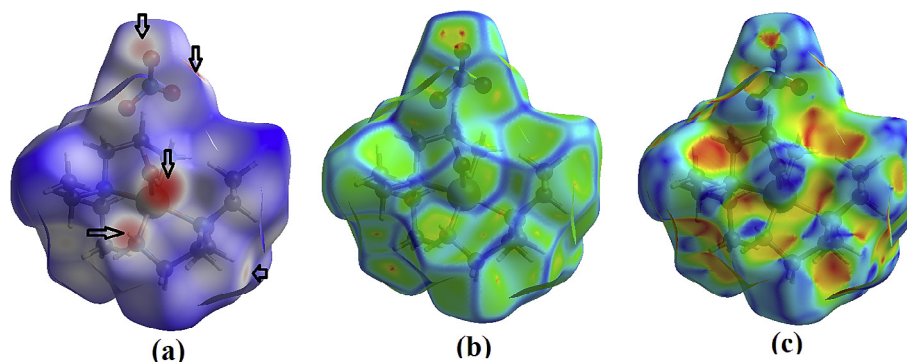
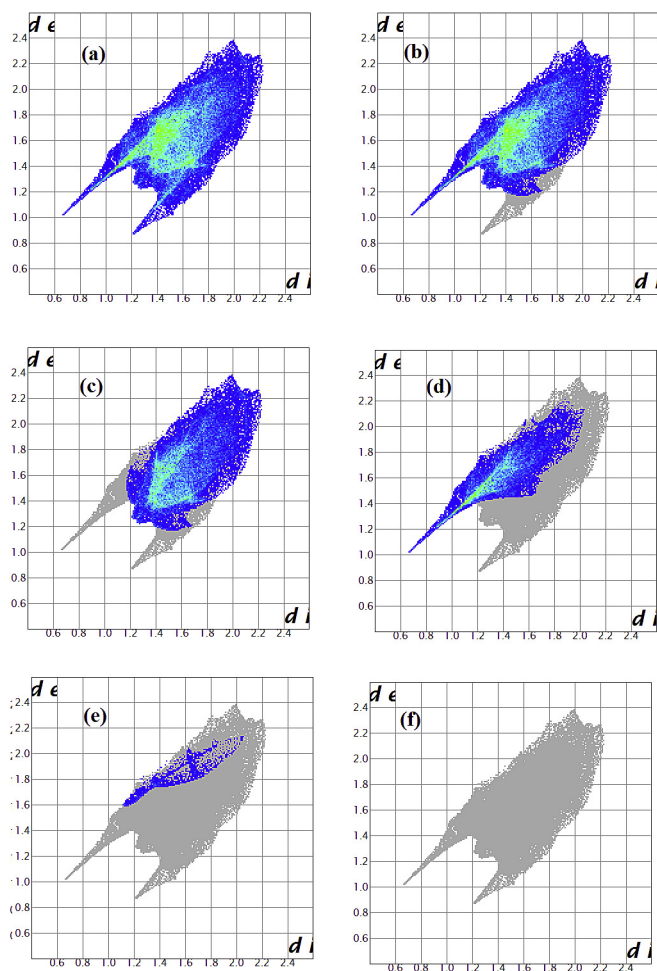Fig. 6. d_{norm} (a), curvedness (b) and shape index (c) mapped on the Hirshfeld surface of complex **2**.

Fig. 7. Fingerprint plots of the complex **2**.

topological coordination of bonds to octahedral geometry depending on their DN donation number ability [49–54].

To explain the solvent effects on the absorption spectra of the complexes, λ_{max} values were plotted against Guttmann's donor values DN as in the solvatochromic (Eq. (1)) and in Fig. 10.

$$\nu_{max} = \nu_{max} + aDN + bAN + c\beta + d\alpha \qquad (1)$$

The solvent parameters used include Guttmann's donor DN, acceptor numbers AN, electron pair donating ability β and hydrogen bonding ability α.

Fig. 10 shows a positive linear relationship between DN values against λ_{max}, which clearly supports the expected Lewis acidity behaviour of such complexes. The bathochromic shifts on λ_{max} of the desired complexes upon increasing DN of solvents are due to the coordination of polar solvents to the square pyramidal Cu(II) centre with different strength, which changed their geometry to octahedral structures [52].

3.7. FTIR spectroscopy

In order to collect the spectroscopic signature of the desired complexes, we performed both experimental and frequency calculation analysis, as seen in Fig. 11. The experimental and theoretical FT-IR vibration spectra of complex **2** in comparison revealed several stretching vibrations corresponding to their expected chemical shifts, as seen in Fig. 11 b and c. Since the calculations was performed for compound in vacuum, while experiment was made for solid; usually, there is a slightly disagreement between observed vibrational and calculated wavenumbers.

The main stretching vibrations chemical shifts belongs to functional groups in complex **2** ($\nu_{(HO-H)}$, $\nu_{(N-H)}$, $\nu_{(C-H)}$, $\nu_{(NO3)}$ and $\nu_{(Cu-N)}$) were compared to their computed frequencies. The metal coordinated water $\nu_{(HO-H)}$ (exp. = 3450 cm^{-1} while DFT = 4000 and 3860 cm^{-1}), diamines $\nu_{(N-H)}$, (exp. = 3250 cm^{-1} while DFT = 3650 and 3460 cm^{-1}), alkyls $\nu_{(C-H)}$ (exp. = 2950 and 2840 cm^{-1} while DFT = 3200 and 3050 cm^{-1}), Nitro $\nu_{(NO3)}$ (exp. = 1450-1250 cm^{-1} while DFT = 1560 cm^{-1}) and metal-N $\nu_{(Cu-N)}$ (exp. ~ 500 cm^{-1} while DFT = 580 cm^{-1}). Generally, the collected results suggested that computed frequencies determined by applying DFT were overestimated their corresponding experimental quantities due to the different anharmonicity and electron correlation effects in the real system [55].

In order to figure out the real IR-relation in such complexes, graphical correlation between the experimental and DFT theoretical analysis was plotted for complex **2**, as is seen in Fig. 11d. A significant R^2 value 0.9931 was collected, which reflected an overall good matching between experimental and theoretical IR analysis. This validates the proposed structure of complex.

3.8. Thermogravimetric analyses

The thermal stability of the complex **2** was performed by TG/DTA. The TGA curves were obtained at a heating rate of 10 °C min^{-1} in open air atmosphere over the temperature range 25−900 °C. The thermogravimetric analyses of these complexes revealed the occurrence of two consecutive processes, namely ligand pyrolysis and inorganic residue formation. The TG/DTA spectra of complex **1** mainly illustrate the expected two steps of weight loss as seen in
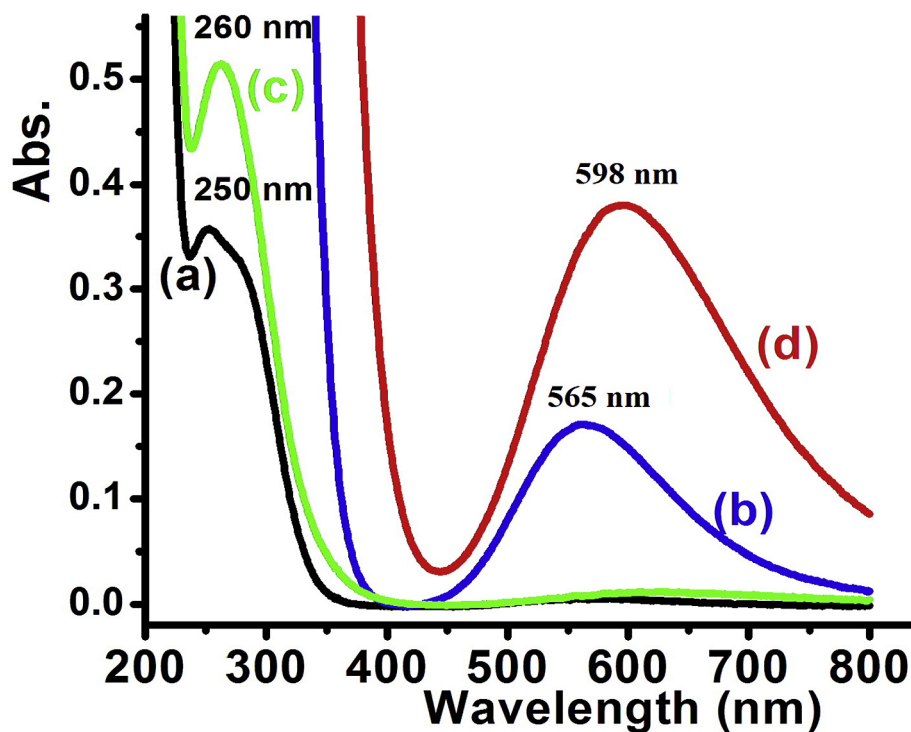
Fig. 8. UV—vis spectra in water at 25 °C of: (a) complex **1** 1×10^{-5} M; (b) complex **1** 1×10^{-4} M; (c) complex **2** 1×10^{-5} M; (d) complex **2** 1×10^{-5} M.

Table 6
Excited sates of complex **2** cation obtained using TDDFT at uBHandH/6-31 + g(2d,p) level of theory.

Excited State	excitation energy (eV)	wavelength (nm)	oscillator strength (f)	S^2
1	1.8332	676.33	0.0004	0.752
2	2.0459	606.01	0.0012	0.752
3	2.1027	589.65	0.0000	0.751
4	2.1358	580.51	0.0000	0.752
5	5.5379	223.88	0.1176	0.799
6	6.0172	206.05	0.0038	0.788
7	6.5375	189.65	0.0714	0.782
8	7.2053	172.07	0.0007	1.238
9	7.3679	168.28	0.0048	0.820
10	7.5270	164.72	0.0076	1.306

Fig. 12. The first decomposition step is a short and simple step due to dehydration of one water molecule at 110 °C. Losing around 3 wt % (theoretically 2.8 wt%), with the exothermic DTA sign at 115 °C. The next step is a more complex one, de-structure of NN and NO_2 ligands and reacting of the Cu centre with O_2 in one broad step starting at 190 °C and ending at 840 °C, losing around 78 wt% (theoretically 77 wt%), with an exothermic DTA sign at 198 °C forming CuO. The final product was identified by IR as copper oxide (CuO, 21 wt%) [25].

3.9. Electrochemical behaviour

An electrochemical analysis for both complexes, **1** and **2**, was perfumed in order to understand their oxidation/reduction behaviour. The experimental data showed that the reduction of complexes proceeds through a quasi-reversible one-electron process with I_{pa}/I_{pc} unity ratio, generating the Cu(I) centre, as illustrated in the general equation and Fig. 13.

$$[Cu^{II}(NN')_2.H_2O](NO_3)_2 \rightleftharpoons [Cu^{I}(NN')_2]NO_3$$

$$E_{1/2} = -0.45 \text{ V for complex } \mathbf{1}$$
$$E_{1/2} = -0.58 \text{ V for complex } \mathbf{2}$$

Fig. 13 shows that the redux potential value ($E_{pa} = -0.63$ V) for complex **2** is slightly more negative compared to that of complex **1** ($E_{pa} = -0.53$ V), which can be attributed to the alkyl functional groups (R_2N), which are considered electron donors. (Et, complex **2**) > (Me, complex **1**) which electronically enriches the Cu(II) centre.

The quasi-reversibility associated with the reduction process probably arises as a consequence of a geometry change from the originally square pyramid towards a distorted tetrahedral environment around the Cu(I) species [25,26].
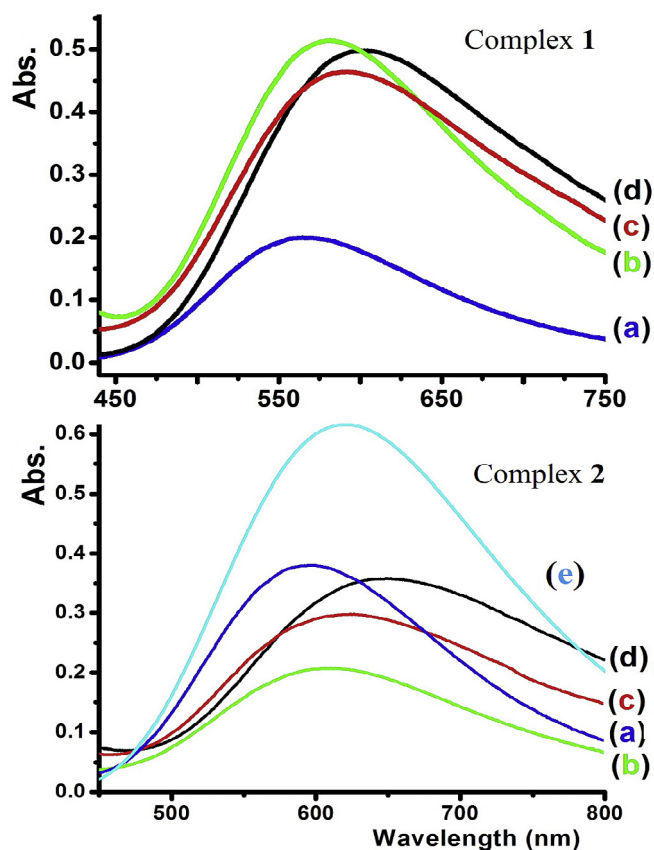
Fig. 9. Absorption spectra of complex **1** in selected solvents, (a) H_2O, $\lambda_{max} = 565$ nm, (b) MeOH, $\lambda_{max} = 573$ nm, (c) DMF, $\lambda_{max} = 592$ nm and (d) DMSO, $\lambda_{max} = 600$ nm and complex **2**, (a) H_2O, $\lambda_{max} = 598$ nm, (b) MeOH, $\lambda_{max} = 604$ nm, (c) DMF, $\lambda_{max} = 627$ nm, (d) DMSO, $\lambda_{max} = 642$ nm and (e) TDDFT theoretical spectrum at uBHandH/6-31 + g(2d,p) level.
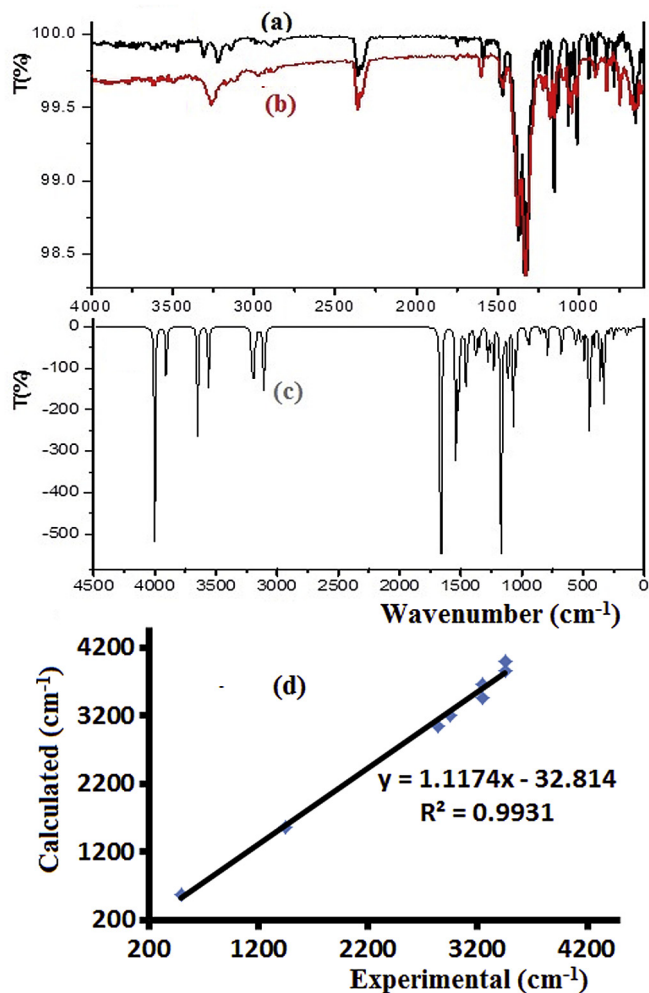
Fig. 11. FT-IR spectra (a) of complex **1**, (b) complex **2** and (c) calculated IR for complex **2** at BHANDH/6-31 + G(2d,p) level of theory and (d) IR-graphical correlation between experimental and DFT analysis.
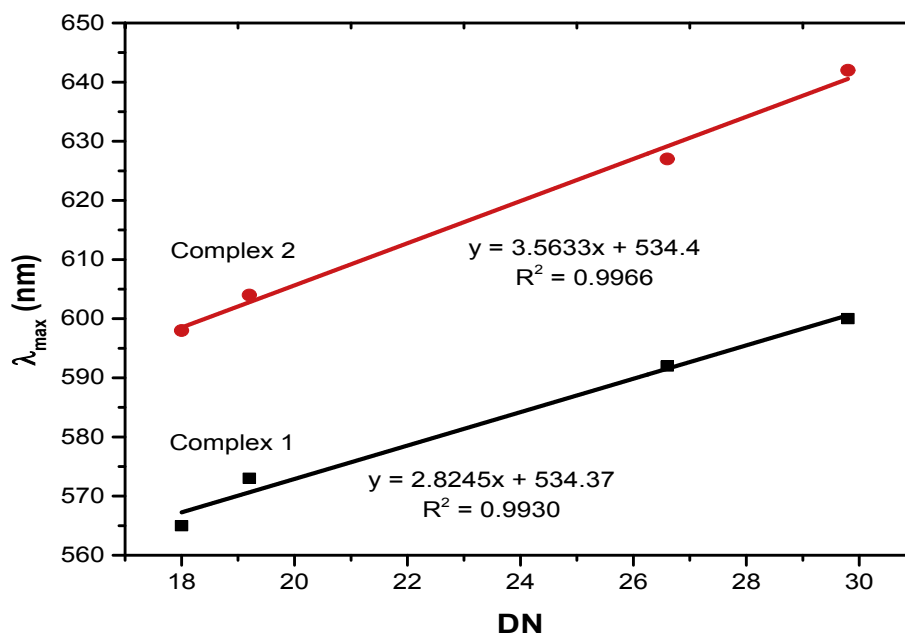
Fig. 10. Correlations of λ_{max} of complexes and DN Guttmann's donor number for solvents.
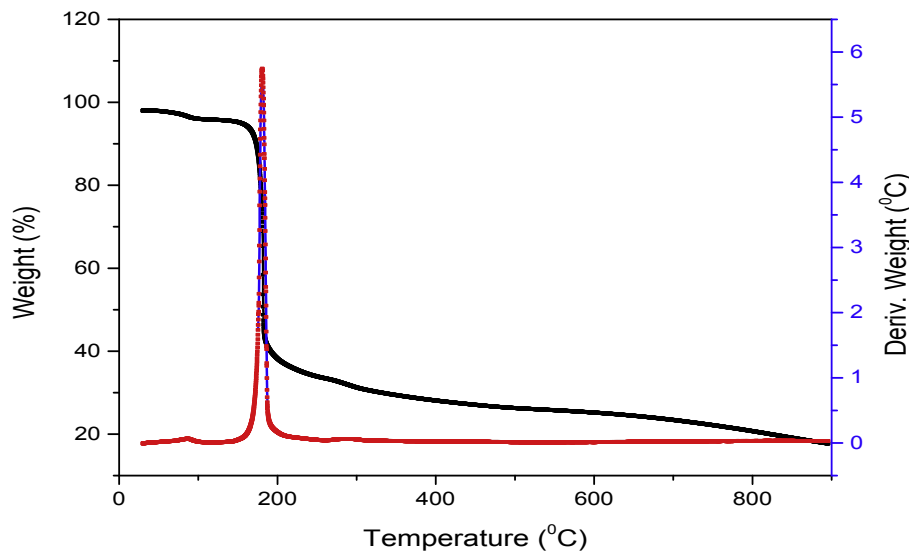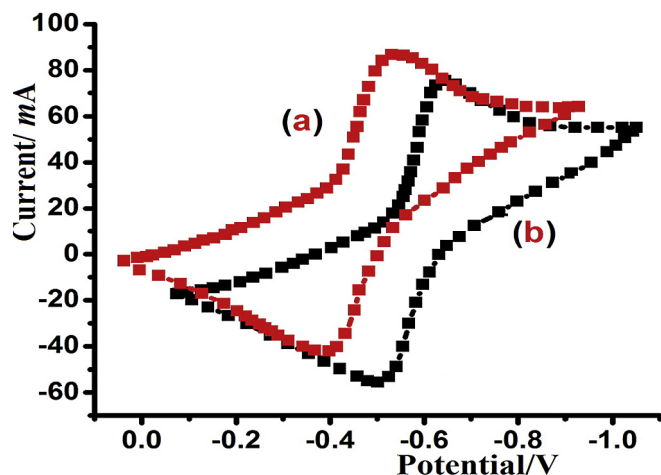
Fig. 12. TG/DTA thermogram of complex **2**.

Fig. 13. Cyclic voltammogram of complex **1** (a) and complex **2** (b) in DMF solution, at scan rates 0.1 V/s.

4. Conclusions

Two new copper(II) complexes were prepared and characterized in this work. The structure of complex **2** was found to have a *trans* penta-coordinated configuration as shown by XRD analysis. Theoretical investigations employing thy BHandH hybrid density functional have agreed with the results obtained from the XRD. The obtained complex in its *trans* conformation was proven to be the most stable as shown form the theoretical study. The Hirshfeld surface analysis indicated the presence of strong intermolecular interactions represented by hydrogen bonds with the O and N atoms. The H-bonds are expected to stabilize the crystal structure of the investigated molecules. The UV spectra of both compounds exhibited visible absorption peaks, which have been attributed to d−d electron transfer. As obtained from the TDDFT calculations performed on complex **2**, it is believed that second excited state at 606 nm is the one responsible for the experimental $\lambda_{\max}$ of complex **2**. The prepared complexes exhibited clear solvatochromism as shown by the UV spectra obtained in different solvents. It was clear that the $\lambda_{\max}$ of both complexes were bathochromic shifted. A Guttmann-type analysis indicated that the reason for the bathochromic shift is due to the coordination of the polar solvents to the square pyramidal Cu(II) centre. The thermal stability of complex **2** was studied by TGA. The complex was found to decompose at two characteristic regions at 115° C and 190 °C. Finally, a cyclic voltammetry investigation on the complexes **1** and **2** indicated a reduction process rising from a geometry transformation from a square pyramidal configuration into a distorted tetrahedral environment.

The biological activity of the copper (II) complexes synthesized in this work will be evaluated in the near future. The antibacterial, antifungal, and anticancer efficiency of the complexes will be investigated *in-vitro*. Also, the complexes will be examined as enzyme inhibitors.

Supplementary material

Crystallographic data for *trans*-[Cu^{II}(NN′)$_2$.H$_2$O](NO$_3$)$_2$ was deposited with the Cambridge Crystallographic Data Centre as supplementary publication number CCDC 1529101. A copy of the XRD information can be obtained free of charge via http://www.ccdc.cam.ac.uk/conts/retrieving.html or from the CCDC, 12 Union Road, Cambridge CB2 1EZ, UK; fax: +44-1223-336033; e-mail: deposit@ccdc.cam.ac.uk.

References

[1] S. Medici, M. Peana, V.M. Nuichi, J.I. Lachowicz, G. Crisponi, M.A. Zoroduu, Coord. Chem. Rev. 284 (2015) 329–350.
[2] A. Li, Y.-H. Liu, L.-Z. Yuan, Z.-Y. Ma, C.-L. Zhao, C.-Z. Xie, W.-G. Bao, J.-Y. Xu, J. Inorg. Biochem. 146 (2015) 52–60.
[3] S. Ebrahimipour, I. Sheikhshoaie, M. Mohamadi, S. Suarez, R. Baggio, M. Khaleghi, M. Torkzadeh-Mahani, A. Mostafavi, Spectrochim. Acta Part A 142 (2015) 410–422.
[4] S.Y. Ebrahimipour, H. Khabazzadeh, J. Castro, I. Sheikhshoaie, A. Crochet, K.M. Fromm, Inorg. Chim. Acta 427 (2015) 52–61.
[5] E. Sundaravadivel, S. Vedavalli, M. Kandaswamy, B. Varghese, P. Madankumar,

RSC Adv. 4 (2014) 40763–40775.
[6] K. Jeyalakshmi, N. Selvakumaran, N.S.P. Bhuvanesh, A. Sreekanth, R. Karvembu, RSC Adv. 4 (2014) 17179–17195.
[7] L. Kelland, Nat. Rev. Cancer 7 (2007) 573–584.
[8] M. Al-Noaimi, A. Nafad, I. Warad, R. Alshwafy, A. Husein, W.H. Talib, T.Ben Hadda, Spectrochim. Acta Part A 122 (2014) 273–282.
[9] A. Zianna, G. Psomas, A. Hatzidimitriou, M. Lalia-Kantouri, RSC Adv. 5 (2015) 37495–37511.
[10] M. Saif, M.M. Mashaly, M.F. Eid, R. Fouad, Spectrochim. Acta Part A 92 (2012) 347–356.
[11] M. Zampakou, N. Rizeq, V. Tangoulis, A.N. Papadopoulos, F. Perdih, I. Turel, G. Psomas, Inorg. Chem. 53 (2014) 2040–2052.
[12] M. Gonzalez-Alvarez, A. Pascual-Alvarez, L.D. Agudo, A. Castineiras, M. Liu-Gonzalez, J. Borras, G. Alzuet-Pina, Dalton. Trans. 42 (2013) 10244–10259.
[13] X.B. Fu, Z.H. Lin, H.F. Liu, X.Y. Le, Spectrochim. Acta Part A 122 (2014) 22–33.
[14] W.-J. Song, Q.-Y. Lin, W.-J. Jiang, F.-Y. Du, Q.-Y. Qi, Q. Wei, Spectrochim. Acta Part A 137 (2014) 122–128.
[15] G. Pratviel, J. Bernadou, B. Meunier, Angew. Chem. Int. Ed. Engl. 34 (1995) 746–769.
[16] A.R. Chakravarty, J. Chem. Sci. 118 (2006) 443–453.
[17] D.D. Li, J.L. Tian, W. Gu, X. Liu, S.P. Yan, J. Inorg. Biochem. 104 (2010) 171–179.
[18] C. Bartel, A.K. Bytzek, Y.Y. Scaffidi-Domianello, G. Grabmann, M.A. Jakupec, C.G. Hartinger, M. Galanski, B.K. Keppler, J. Inorg. Biochem. 17 (2012) 465–474.
[19] M. Al-Noaimi, M. Suleiman, H.W. Darwish, A.H. Bakheit, M. Abdoh, Iyad Saadeddin, N. Shivalingegowda, N.K. Lokanath, O. Bsharat, A. Barakat, I. Warad, Bioinorg. Chem. Appl. 7 (2014) 2014.
[20] T. Kiran, V.G. Prasanth, M.M. Balamurali, C.S. Vasavi, P. Munusami, K.I. Sathiyanarayanan, M. Pathak, Inorg. Chim. Acta 433 (2015) 26–34.
[21] S. Tabassum, S. Amir, F. Arjmand, C. Pettinari, F. Marchetti, N. Masciocchi, G. Lupidi, R. Pettinari, Eur. J. Med. Chem. 60 (2013) 216–232.
[22] T. Suzuki, S. Kitamura, R. Khota, K. Sugihara, N. Fujimoto, S. Ohta, Toxicol. Appl. Pharmacol. 203 (2005) 9–17.
[23] Y.S. Mary, P.J. Jojo, C.Y. Panicker, C.V. Alsenoy, S. Ataei, I. Yildiz, Spectrochim. Acta Part A 122 (2014) 499–511.
[24] A. Cassol, P. Di Bernardo, R. Portanova, M. Tolazzi, G. Tomat, P. Zanonato, J. Chem. Soc. Dalton Trans. (1992) 469–474.
[25] M. Al-Noaimi, M.I. Choudhar, F.F. Awwadi, W.H. Talib, T. Ben Hadda, S. Yousuf, A. Sawafta, I. Warad, Spectrochim. Acta Part A 127 (2014) 225–230.
[26] F. Abu Saleemh, S. Musameh, A. Sawafta, P. Brandao, C.J. Tavares, S. Ferdov, A. Barakat, A. Al Ali, M. Al-Noaimi, I. Warad, Arab. J. Chem. (2016), http://dx.doi.org/10.1016/j.arabjc.2016.10.008.
[27] Bruker SAINT-plus, Bruker AXS Inc., Madison, Wisconsin, USA, 2007.
[28] G.M. Sheldrick, SADABS, University of Göttingen, Germany, 1996.
[29] G.M. Sheldrick, Acta Cryst. A64 (2008) 112.
[30] O.V. Dolomanov, L.J. Bourhis, R.J. Gildea, J.A.K. Howard, H. Puschmann, J. Appl. Cryst. 42 (2009) 339–341.
[31] M. Atanasov, P. Comba, B. Martin, V. Müller, G. Rajaraman, H. Rohwer, S. Wunderlich, J. Comp. Chem. 27 (2006) 1263–1277.
[32] I. Badran, N.N. Nassar, N.N. Marei, A. Hassan, RSC Adv. 6 (2016) 54418–54430.
[33] I. Badran, A. Rauk, Y.J. Shi, J. Phys. Chem. 116 (2012) 11806–11816.
[34] A. Becke, Phys. Rev. B 33 (1986) 8822–8824.
[35] A.D. Becke, J. Phys. Chem. 98 (1993) 1372–1377.
[36] F. Weigend, Phys. Chem. Chem. Phys. 8 (2006) 1057–1065.
[37] A.P. Scott, L. Radom, J. Phys. Chem. 100 (1996) 16502–16513.
[38] M. Frisch, G.W. Trucks, H. Schlegel, G.E. Scuseria, M.A. Robb, J.R. Cheeseman, J.M. Millam, Gaussian 03, Revision c. 02, Gaussian. Inc., Wallingford, CT, 2004, p. 4.
[39] S.K. Wolff, D.J. Grimwood, J.J. McKinnon, D. Jayatilaka, M.A. Spackman, Crystal explorer 2.1, University of Western Australia, Perth (, 2007.
[40] P. Naumov, K. Sakurai, A. Nukui, M. Tanaka, Chem. Commun. (2007) 347–349.
[41] A.W. Addison, T.N. Rao, J. van, R. Reedijk, G.C. Verschoor, J. Chem. Soc. Dalton Trans. (1984) 1349.
[42] CSD Cambridge Database, 2015, 1.18.
[43] J.S. Binkley, J.A. Pople, Inter. J. Quant. Chem. 9 (1975) 229–236.
[44] M.A. Spackman, D. Jayatilaka, CrystEngComm 11 (2009) 19–32.
[45] M.A. Spackman, J.J. McKinnon, CrystEngComm 4 (2002) 378–392.
[46] I. Warad, F. Al-Rimawi, A. Barakat, S. Affouneh, N. Shivalingegowda, N.K. Lokanath, I.M. Abu-Reidah, Chem. Cent. J. 10 (2016) 38.
[47] I. Warad, A. Barakat, J. Mol. Struct. 1134 (2017) 17–24.
[48] I. Warad, Y. Al-Demeri, M. Al-Nuri, S. Shahwan, M. Abdoh, Sh. Naveen, N.K. Lokanath, M.S. Mubarak, T. Ben Hadda, Y.N. Mabkhot, J. Mol. Struct. 1142 (2017) 217–225.
[49] H. Golchoubian, H. Ghorbanpour, E. Rezaee, Inorg. Chim. Acta 442 (2016) 30–36.
[50] H. Golchoubian, E. Rezaee, G. Bruno, H.A. Rudbari, Inorg. Chim. Acta 366 (2011) 290–297.
[51] I. Warad, F.F. Awwadi, M. Daqqa, A. Al Ali, T.S. Ababneh, T.M.A. AlShboul, T.M.A. Jazzaz, F. Al-Rimawi, T. Ben Hadda, Y.N. Mabkhot, J. Photochem. Photobiol. B Biol. 171 (2017) 9–19.
[52] G.V. Baryshnikov, B.F. Minaev, A.A. Baryshnikova, H. Ågren, Chem. Phys. Let. 661 (2016) 48–52.
[53] G.V. Baryshnikov, B.F. Minaev, A.A. Baryshnikova, H. Ågren, Chem. Phys. 491 (2017) 48–55.
[54] A.T. Baryshnikova, B.F. Minaev, G.V. Baryshnikov, W.-H. Sun, Russ. J. Inorg. Chem. 61 (2016) 588–593.
[55] A. Atac, C. Karaca, S. Gunnaz, M. Karabacak, Spectrochim. Acta A 130 (2014) 516–525.